

TSL/ISV-98-0198  
October 1998

## Higher Partial Waves in $pp \rightarrow pp\eta$ near Threshold

H. Calén <sup>a</sup>, J. Dyring <sup>a</sup>, G. Fäldt <sup>a</sup>, K. Fransson <sup>a</sup>, L. Gustafsson <sup>a</sup>, S. Häggström <sup>a</sup>,  
B. Höistad <sup>a</sup>, J. Johanson <sup>a</sup>, A. Johansson <sup>a</sup>, T. Johansson <sup>a</sup>, S. Kullander <sup>a</sup>,  
A. Mörtsell <sup>a</sup>, R. Ruber <sup>a</sup>, J. Złomańczuk <sup>a</sup>, C. Ekström <sup>b</sup>, K. Kilian <sup>c</sup>, W. Oelert <sup>c</sup>,  
T. Sefzick <sup>c</sup>, R. Bilger <sup>d</sup>, W. Brodowski <sup>d</sup>, H. Clement <sup>d</sup>, G.J. Wagner <sup>d</sup>, A. Bondar <sup>e</sup>,  
A. Kuzmin <sup>e</sup>, B. Shwartz <sup>e</sup>, V. Sidorov <sup>e</sup>, A. Sukhanov <sup>e</sup>, V. Dunin <sup>f</sup>, B. Morosov <sup>f</sup>,  
A. Povtorejko <sup>f</sup>, A. Sukhanov <sup>f</sup>, A. Zernov <sup>f</sup>, A. Kupsc <sup>g</sup>, P. Marciniwski <sup>g</sup>,  
J. Stepaniak <sup>g</sup>, J. Zabierowski <sup>h</sup>, A. Turowiecki <sup>i</sup>, Z. Wilhelmi <sup>i</sup>, C. Wilkin <sup>j</sup>

<sup>a</sup> Department of Radiation Science, Uppsala University, S-751 21 Uppsala, Sweden

<sup>b</sup> The Svedberg Laboratory, S-751 21 Uppsala, Sweden

<sup>c</sup> IKP, Forschungszentrum Jülich GmbH, D-52425 Jülich, Germany

<sup>d</sup> Physikalisches Institut, Tübingen University, D-72076 Tübingen, Germany

<sup>e</sup> Institute of Nuclear Physics, Novosibirsk 630 090, Russia

<sup>f</sup> Joint Institute for Nuclear Research Dubna, 101000 Moscow, Russia

<sup>g</sup> Institute for Nuclear Studies, PL-00681 Warsaw, Poland

<sup>h</sup> Institute for Nuclear Studies, PL-90137 Łódź, Poland

<sup>i</sup> Institute of Experimental Physics, Warsaw University, PL-0061 Warsaw, Poland

<sup>j</sup> Physics & Astronomy Dept., University College London, London WC1E 6BT, U.K.

**Abstract:** Exclusive measurements of the production of  $\eta$ -mesons in the  $pp \rightarrow pp\eta$  reaction have been carried out at excess energies of 16 and 37 MeV above threshold. The deviations from phase space are dominated by the proton-proton final state interaction and this influences particularly the energy distribution of the  $\eta$  meson. However, evidence is also presented at the higher energy for the existence of an anisotropy in the angular distributions of the  $\eta$ -meson and also of the final proton-proton pair, probably to be associated with  $D$ -waves in this system interfering with the dominant  $S$ -wave term. The sign of the  $\eta$  angular anisotropy suggests that  $\rho$ -exchange is important for this reaction.

The production of  $\eta$  mesons in proton-proton collisions near threshold has been measured in recent years by three different groups [1, 2, 3] and a fairly consistent picture has emerged. In comparison to the analogous pion case [4, 5],  $S$ -wave production is more dominant near threshold, and this is generally ascribed to the presence of the  $N^*(1535) S_{11}$  isobar, whose width overlaps the  $\eta - p$  threshold and which has large branching fractions into both  $\eta - p$  and  $\pi - p$  [6]. Dalitz plots obtained for the  $pp \rightarrow pp\eta$  reaction at low energy show strong deviations from phase space due to the presence of the proton-proton final state interaction (FSI) [3]. In addition there are residual effects but the precision of these measurements was limited, in part, by the uncertainty in the determination of the proton angles. This defect has been overcome in the present experiment through the inclusion of a tracking device covering the forward angles and operating in conjunction with the apparatus previously used. The combination allowed us to investigate the influence of higher partial waves in the angular distributions and to identify dependences on both the angles of the  $\eta$  and of the proton-proton relative momentum, which become stronger with energy. This behaviour is the first indication of effects from higher partial waves in the  $pp \rightarrow pp\eta$  reaction. The shape of the  $\eta$  angular variation is sensitive to the basic production mechanism and the data suggest that  $\rho$ -exchange provides a more important driving term here than  $\pi$ -exchange.

The experiment was carried out using the PROMICE/WASA facility at the CELSIUS storage ring of the The Svedberg Laboratory at beam energies of 1296 and 1350 MeV, corresponding to centre-of-mass excess energies  $Q = 16$  and 37 MeV respectively. Using a cluster gas jet target, integrated luminosities of about  $50 \text{ nb}^{-1}$  and  $200 \text{ nb}^{-1}$  were obtained for the two energies in a total of 30 hours of running, and these yielded about 300 and 750 good  $pp\eta$  events in the final sample. Details of the detector system are given in Refs. [7, 8], and only the main points are discussed here.

The forward-going protons were measured in a detector system covering polar angles between  $4^\circ$  and  $20^\circ$  with respect to the beam direction. It consists of a tracking detector, followed by a three-layer scintillator hodoscope and a four-layer scintillator calorimeter. A second hodoscope is placed at the end of the detector system to register penetrating particles. The tracker consists of two planes, each with four layers of thin-walled cylindrical drift

chambers, so-called “straw chambers”, oriented in the vertical and horizontal directions. This arrangement allows the proton scattering angles to be reconstructed to a precision of better than  $1^\circ$  (FWHM). The  $\eta$ 's are identified from their  $2\gamma$  decay channel, where the  $\gamma$ 's are detected in two CsI(Na) arrays situated on either side of the scattering chamber. Scintillator hodoscopes are placed in front of the CsI arrays to veto charged particles. The  $2\gamma$  invariant mass resolution obtained at the  $\eta$ -meson mass is 20 MeV (RMS).

In the off-line analysis, only those events with an identified  $\eta$  meson together with two energetic protons in the forward detector were retained and, in these cases, a kinematical fit was applied in order to extract the energy-momentum vectors for the particles. To avoid problems in accounting for losses through nuclear reactions in the detector material, only the proton directions were used, and this results in a fit with three constraints (3C). The number of background events with two uncorrelated  $\gamma$ 's arising from different pions in  $2\pi^0$  production becomes negligible after applying a lower cut at 5% on the confidence level of the fit. In the subsequent analysis of our data, we exploit the fact that at low energies only a few amplitudes are allowed and that these lead to distributions in which the angular and momentum variables are intimately linked. It is only through the introduction of such a functional form into Monte Carlo simulations that we can draw any firm conclusions on the physics of the process. The detector response and acceptance calculations for the experiment were made with events generated from a full Monte Carlo simulation using GEANT3 [9]. The resulting geometrical acceptance for this type of event is about 0.5% and 2% at  $Q = 16$  and 37 MeV respectively. The data were checked for internal consistency by applying different geometrical cuts.

The sole production amplitude which survives at threshold corresponds to the transition  ${}^3P_0 \rightarrow {}^1S_0 s$ , where we are using the standard  ${}^{2S+1}L_J$  notation for the  $pp$  system, with the lower case letter denoting the angular momentum of the  $\eta$ -meson with respect to the  $pp$  system. At slightly higher energies, amplitudes corresponding to the production of  $P$ - and  $D$ -wave  $pp$  pairs introduce dependences on the  $pp$  angles with similar momentum threshold factors since the  $D$ -wave term can interfere with the threshold  $S$ -wave amplitude. However, given that  $\eta$  production in the  ${}^1S_0 p$  state is forbidden by selection rules, the first non-trivial  $\eta$  angular dependence is expected to come from the interference of the  $s$ - and

$d$ -wave amplitudes. These considerations lead us to take the following simple form for the low energy  $pp \rightarrow pp\eta$  amplitude:

$$M = \tilde{A}_{Ss} \phi_f^\dagger(\hat{p} \cdot \vec{\varepsilon}_i) + A_{Sd} \phi_f^\dagger(\hat{p} \cdot \vec{k})(\vec{k} \cdot \vec{\varepsilon}_i) + A_{Ps} \phi_i(\vec{q} \cdot \vec{\varepsilon}_f^\dagger) + A_{Ds} \phi_f^\dagger(\hat{p} \cdot \vec{q})(\vec{q} \cdot \vec{\varepsilon}_i). \quad (1)$$

The momenta of the initial proton and final  $\eta$  in the overall c.m. system are denoted by  $\vec{p}$  and  $\vec{k}$  respectively,  $2\vec{q}$  is the relative momentum in the final two-proton system,  $\vec{\varepsilon}_i$  ( $\vec{\varepsilon}_f$ ) the spin-one polarisation vector of the initial (final) proton-proton pair, and  $\phi_i$  ( $\phi_f$ ) the corresponding spin-zero functions. The indices on the amplitudes denote the dominant final angular momentum state in a term. It should however be noted that the strict  $Ss$  partial wave amplitude is given by

$$A_{Ss} = \tilde{A}_{Ss} + \frac{1}{3} k^2 A_{Sd} + \frac{1}{3} q^2 A_{Ds}. \quad (2)$$

Keeping only terms up to order  $k^2$  or  $q^2$ , *i.e.* a total of two units of angular momentum in the final intensity, the spin-averaged matrix element squared becomes

$$\overline{|M|^2} = \frac{1}{4} \left[ |\tilde{A}_{Ss}|^2 + 2k^2 \operatorname{Re} \left\{ \tilde{A}_{Ss}^* A_{Sd} \right\} \cos^2 \theta_\eta + 2q^2 \operatorname{Re} \left\{ \tilde{A}_{Ss}^* A_{Ds} \right\} \cos^2 \theta_{pp} + q^2 |A_{Ps}|^2 \right], \quad (3)$$

where  $\theta_\eta$  and  $\theta_{pp}$  are the angles that the  $\eta$  and the  $pp$  relative momentum make with respect to the beam direction.

In a model where the  $N^*(1535)$  isobar is excited through one pion exchange [10], it is expected that the  $|A_{Ps}|^2$  term should be smaller than the  $\operatorname{Re} \left\{ \tilde{A}_{Ss}^* A_{Ds} \right\}$  of the  $Ss$ - $Ds$  interference by a factor of the order of  $\mu/4m_p$ , where  $m_\eta$  and  $m_p$  are the  $\eta$  and proton masses respectively, and  $\mu = 2m_p m_\eta / (2m_p + m_\eta)$  is the reduced mass of the final state. Since the  $Ps$  term has no characteristic angular dependence, it would be difficult to isolate a small effect as compared to a possible energy dependence of  $\tilde{A}_{Ss}$ , and so any such contribution is ignored.

The  ${}^1S_0$  state of the final  $pp$  system is subject to a very strong FSI which is central to any analysis of low energy production. All the terms in Eq. (3) are influenced by the FSI, with the exception of the  $P$ -wave contribution, and this will reduce even further the relative importance of  $|A_{Ps}|^2$ . Without knowing the radial dependence of the  $\eta$ -production operator, the FSI effect is slightly model-dependent. We estimate it by taking the ratio of

the Paris  ${}^1S_0$  wave function [11] at its maximum at  $r = 1$  fm to the corresponding plane wave function; numerical calculations with the Paris wave functions show that Coulomb effects are negligible under the conditions of the present experiment. There is a common enhancement factor  $F_{SS}(q)$  for the  $(SS)^2$  and  $Ss-Sd$  interference terms and an analogous  $F_{SD}(q)$  for the  $Ss-Ds$  interference. They may be parametrised in a similar manner to that given in ref. [12]

$$\begin{aligned} F_{SS}(q) &= 0.440 + \frac{151.7}{1 + q^2/\alpha^2}, \\ F_{SD}(q) &= 0.968 + \frac{11.5}{1 + q^2/\alpha^2}, \end{aligned} \quad (4)$$

with  $\alpha = -0.053 \text{ fm}^{-1}$ .

We make the assumption that, apart from the FSI, the amplitudes  $\tilde{A}_{Ss}$ ,  $A_{Sd}$  and  $A_{Ds}$  appearing in Eq. (3) are constant. The resulting form of the differential cross section is

$$d\sigma = \frac{N}{p} \left( F_{SS}(q) + a \frac{k^2}{\mu m_p} F_{SS}(q) \cos^2 \theta_\eta + b \frac{q^2}{\mu m_p} F_{SD}(q) \cos^2 \theta_{pp} \right) dLips, \quad (5)$$

where  $N$  is a normalization constant and  $dLips$  is the invariant three-body phase space distribution. Typical momentum factors  $\mu m_p$  are explicitly shown to leave two dimensionless constants  $a$  and  $b$  to be determined from the shapes of the angular and energy distributions. It must be stressed that the functional form of Eq. (5) does not depend upon the details of a specific dynamical model but on the assumption of constant amplitudes.

To extract differential distributions from the data, we fitted the Monte Carlo simulations, with events weighted according to Eq. (4), to the experimental results. Following this procedure at  $Q = 37$  MeV, a combined fit to the  $\theta_\eta$  and  $\theta_{pp}$  angular distributions yields the parameter values  $a = -15 \pm 5$  and  $b = 22 \pm 7$ , which are correlated, and the overall normalisation constant. In addition to the given statistical errors, there are systematic errors, arising mainly from uncertainties in the geometrical alignment of the apparatus, which are of the order 10% for the  $a$  parameter and 20% for the  $b$  parameter. These values were then used in the Monte Carlo simulation to make the acceptance corrections needed to unfold the data; the resulting corrected experimental data and fitted angular distributions are shown in Figs. 1a and 2a. It should be noted that the  $a$  and  $b$  parameters were not deduced by fitting to the corrected data shown in the figures.

The distribution in the  $\eta$  kinetic energy  $T_\eta$ , shown in Fig. 3a, is shifted towards higher energies with respect to phase space. This is a direct consequence of the strongly attractive  $pp$  FSI, which enhances events where the  $\eta$  recoils against the two protons which have low excitation energy. The dashed curve, which corresponds to phase space modified by the FSI, produces too big an effect. The solid curve is the prediction with the values of  $a$  and  $b$  as determined by the angular distributions. The non-vanishing of the averages of  $\cos^2 \theta$  leaves  $k^2$  and  $q^2$  terms in Eq. (5) which yield a much better fit.

At  $Q = 16$  MeV, S-waves are even more dominant and the angular distributions are broadly compatible with phase space modified by the  $pp$  FSI. Nevertheless the shapes are in fact marginally better reproduced with the parameter values derived from the higher energy data and the corresponding predictions are shown in Figs. 1b and 2b. The  $T_\eta$  data shown in Fig. 3b, while again demonstrating the effect of the  $pp$  FSI, are well described by the parametrisation. The experimental points do depend, to some extent, on the shape of the assumed differential distribution, but this is well within the statistical uncertainty of the data. The poor quality of the data for  $\cos \theta_{pp} > 0.8$  and at the upper end of the  $T_\eta$  distribution reflects mainly the loss of events due to the beam pipe so that discrepancies with the parametrisation should not be taken seriously in these regions.

The numerical values of the differential cross sections are given in Tables 1–3. The data were normalised to the values of the total  $pp \rightarrow pp\eta$  cross sections given in Ref. [3], namely  $\sigma(T_p = 1293 \text{ MeV}) = (2.11 \pm 0.32) \mu\text{b}$  and  $\sigma(T_p = 1352 \text{ MeV}) = (4.92 \pm 0.74) \mu\text{b}$ .

All existing theoretical models describing  $\eta$ -production in proton-proton scattering are broadly similar [10, 13], consisting of a meson exchange exciting a nucleon isobar, dominantly the  $S_{11}$   $N^*(1535)$ , which decays into an  $s$ -wave  $\eta$ -proton pair. The models differ mainly in their choice of mesons exchanged and, in particular, the relative importance of  $\pi$  and  $\rho$  exchange [10, 13]. If, for simplicity, only the pion exchange term is retained then it follows from the expansion of the corresponding propagator and vertex function that  $a = 1$  and  $b = 4$  [14]. Our experimental values are significantly larger than these.

Higher partial wave  $N^*$  resonances are potentially very important for the  $\eta$  angular distribution. Away from threshold there is evidence for significant  $d$ -wave production of the  $\eta$  meson in the  $\pi^- p \rightarrow \eta n$  reaction [15] and this is confirmed in the preliminary high

statistics data from the Crystal Ball collaboration [16]. Whilst having no appreciable effect on the  $pp$  angular distribution, the inclusion of such  $d$ -wave production in a one pion exchange model would contribute about  $a \approx +7$  in the  $\eta$  angular distribution which, though of the right order of magnitude, is of opposite sign to what we have deduced from our data. Thus, in contrast to our findings presented in Fig. 1b, such a term would favour production towards  $\cos\theta_\eta = \pm 1$ .

However the sign of the  $\cos^2\theta_\eta$  term is negative in the photoproduction  $\gamma p \rightarrow \eta p$  a little above threshold [17] and, using vector dominance ideas, this is likely to be true for  $pp \rightarrow \eta p$  as well. In a pure  $\rho$ -exchange model, the elementary distribution would contribute  $a \approx -2.5$  which, though too small, is of the same sign as the one apparent in our data. In the original estimation of this process [10] it was claimed that  $\rho$ -exchange should be stronger than  $\pi$ -exchange and that the interference between them was mainly destructive. If this were indeed the case, the  $a$  coefficient could be enhanced significantly because of the negative sign between the  $\rho$  and  $\pi$  amplitudes. Our data would support such a conclusion. This would also lead to the prediction that the  $pn \rightarrow d\eta$  should show a much flatter distribution since the  $\rho$  and  $\pi$  amplitudes add in this case [10].

In conclusion, we have presented the first experimental evidence for non-isotropy in the  $pp \rightarrow pp\eta$  angular distributions close to threshold. The signals are generally small in the data as compared for example to the proton-proton final state interaction, which has overwhelming importance. Nevertheless, a clear sign of an  $\eta$  angular anisotropy has been found which could be the first direct indication of  $\rho$ -dominance in  $\eta$  production.

An economic description of all our distributions, sufficient for acceptance corrections, has been given in terms of the two free parameters of Eq. (5) by taking the amplitudes  $\tilde{A}_{Ss}$ ,  $A_{Sd}$  and  $A_{Ds}$  to be constant. If, for example, we assume instead that  $A_{Ss}$  of Eq. (2) is constant then the  $\cos^2\theta$ 's in Eq. (5) are replaced by Legendre polynomials  $P_2(\cos\theta)$ . The fits to the angular distributions in Figs. 1 and 2 are very similar but, due to the vanishing of the angular average of  $P_2(\cos\theta)$ , the results in Fig. 3 are identical to the broken curve, which represents just phase space and FSI. To restore the previous good agreement requires an additional free  $q^2$  or  $k^2$  term in the fitting and, when this is introduced, the results are essentially identical to the solid curve of Fig. 3. The shapes of the angular distributions

are unaffected by such a modified procedure.

A significant improvement of the statistics would be welcome to tie down the model parameters in this area. Such an improvement is anticipated through the use of the WASA detector [18], which is designed for the study of rare decays of the  $\eta$  meson and which will have an almost  $4\pi$  coverage of the photons from the  $\eta$  decay. The effects of higher partial waves should increase strongly with beam energy but to exploit this would, in our case, require an energy upgrade of CELSIUS or the study of quasi-free production on the deuteron.

We are grateful to the TSL/ISV personnel for their continued help during the course of this work. Discussions with M. Garçon on the analysis of this experiment were very helpful. Financial support for this experiment and its analysis was provided by the Swedish Natural Science Research Council, the Swedish Royal Academy of Science, the Swedish Institute, the Bundesministerium für Bildung und Forschung (06TU886), Deutsche Forschung Gesellschaft (Mu 705/3 Graduiertenkolleg), the Polish State Committee for Scientific Research, the Russian Academy of Science, and the European Science Exchange Programme. The data presented here are based upon the work of J. Dyring, in partial fulfillment of the Ph.D. requirements [8].



## References

- [1] A.M. Bergdolt et al., Phys. Rev. **D48** (1993) R2969; F. Hibou et al., Phys. Lett. **B438** (1998) 41
- [2] E. Chiavassa et al., Phys. Lett. **B322** (1994) 270.
- [3] H. Calén et al., Phys. Lett. **B366** (1996) 39; U. Schuberth, PhD thesis (University of Uppsala), Acta Universitatis Upsaliensis **5**, 1995.
- [4] H.O. Meyer et al., Phys. Rev. Lett. **65** (1990) 2846; *ibid* Nucl. Phys. **B539** (1992) 633.
- [5] A. Bondar et al., Phys. Lett. **B356** (1995) 8.
- [6] C. Caso et al., Eur. Phys. J. **C3** (1998) 1.
- [7] H. Calén et al., Nucl. Instr. Meth. **A379** (1996) 57.
- [8] J. Dyring, PhD thesis (University of Uppsala), Acta Universitatis Upsaliensis **14**, 1997.
- [9] GEANT-Detector Description and Simulation Tool, CERN Program Library long write-up W5013, CERN (1993).
- [10] J.-F. Germond and C. Wilkin, Nucl. Phys. **A518** (1990) 308.
- [11] M. Lacombe, B. Loiseau, J.M. Richard, R. Vinh Mau, F. Côté, P. Pirès, and R. de Tourreil, Phys. Rev. **C21** (1980) 861; B. Loiseau (private communication).
- [12] G. Fäldt and C. Wilkin, Phys. Lett. **B382** (1996) 209; *ibid* Phys. Rev. **C56** (1997) 2067.
- [13] T. Vetter, A. Engel, T. Biró, and U. Mosel, Phys. Lett. **B263** (1991) 153; J.M. Laget, F. Wellers and J.F. Lecomte, Phys. Lett. **B257** (1991) 254; M. Batinić, A. Švarc, and T.-S.H. Lee, Physica Scripta **56** (1997) 321; A. Moalem, E. Gedalin, L. Razdolskaya, and Z. Shorer, Nucl. Phys. **A600** (1996) 445.
- [14] G. Fäldt and C. Wilkin (unpublished).
- [15] W. Deinet et al., Nucl. Phys. **B11** (1969) 495.
- [16] B.M.K. Nefkens (private communication).
- [17] B. Krusche et al. Phys. Rev. Lett. **74** (1995) 3736; *idem* **75** (1995) 3023; Z. Phys. **A351** (1995) 237.

- [18] S. Kullander, Proc. 14th Int. Conf. on Particles and Nuclei, (World Scientific, Singapore, 1997), p.754.

Table 1: Differential cross section with respect to the  $\eta$  c.m. angle for the  $pp \rightarrow pp\eta$  reaction at  $Q = 16$  and  $37$  MeV ( $T_p = 1296$  and  $1350$  MeV). In addition to the statistical error, there is an overall systematic uncertainty of about 20%.

$Q = 16$ MeV		$Q = 37$ MeV	
$\cos \theta_\eta$	$d\sigma/d\Omega_\eta$ ( $\mu\text{b}/\text{sr}$ )	$\cos \theta_\eta$	$d\sigma/d\Omega_\eta$ ( $\mu\text{b}/\text{sr}$ )
-0.9	$0.170 \pm 0.029$	-0.9	$0.234 \pm 0.027$
-0.7	$0.168 \pm 0.033$	-0.7	$0.317 \pm 0.040$
-0.5	$0.123 \pm 0.029$	-0.5	$0.392 \pm 0.049$
-0.3	$0.219 \pm 0.039$	-0.3	$0.552 \pm 0.061$
-0.1	$0.186 \pm 0.036$	-0.1	$0.479 \pm 0.057$
0.1	$0.262 \pm 0.044$	0.1	$0.490 \pm 0.057$
0.3	$0.164 \pm 0.032$	0.3	$0.434 \pm 0.060$
0.5	$0.157 \pm 0.031$	0.5	$0.554 \pm 0.069$
0.7	$0.178 \pm 0.034$	0.7	$0.425 \pm 0.061$
0.9	$0.100 \pm 0.024$	0.9	$0.188 \pm 0.038$

Table 2: Differential cross section with respect to the proton-proton angle for the  $pp \rightarrow pp\eta$  reaction at  $Q = 16$  and  $37$  MeV. In addition to the statistical error, there is an overall systematic uncertainty of about 20%.

$Q = 16$ MeV		$Q = 37$ MeV	
$\cos \theta_{pp}$	$d\sigma/d\Omega_{pp}$ ( $\mu\text{b}/\text{sr}$ )	$\cos \theta_{pp}$	$d\sigma/d\Omega_{pp}$ ( $\mu\text{b}/\text{sr}$ )
0.05	$0.196 \pm 0.039$	0.05	$0.331 \pm 0.043$
0.15	$0.150 \pm 0.029$	0.15	$0.308 \pm 0.041$
0.25	$0.166 \pm 0.028$	0.25	$0.343 \pm 0.043$
0.35	$0.182 \pm 0.026$	0.35	$0.405 \pm 0.047$
0.45	$0.169 \pm 0.024$	0.45	$0.344 \pm 0.042$
0.55	$0.190 \pm 0.029$	0.55	$0.355 \pm 0.042$
0.65	$0.125 \pm 0.029$	0.65	$0.473 \pm 0.050$
0.75	$0.163 \pm 0.043$	0.75	$0.391 \pm 0.050$
0.85	$0.169 \pm 0.084$	0.85	$0.508 \pm 0.070$
—	—	0.95	$0.88 \pm 0.19$

Table 3: Differential cross section with respect to the  $\eta$  c.m. kinetic energy for the  $pp \rightarrow pp\eta$  reaction at  $Q = 16$  and  $37$  MeV. In addition to the statistical error, there is a typical systematic uncertainty of about 20%, which increases at the upper end of the spectrum.

$Q = 16$ MeV		$Q = 37$ MeV	
$T_\eta$	$d\sigma/dT_\eta$ ( $\mu\text{b}/\text{MeV}$ )	$T_\eta$	$d\sigma/dT_\eta$ ( $\mu\text{b}/\text{MeV}$ )
0.5	$0.046 \pm 0.010$	1.0	$0.055 \pm 0.010$
1.5	$0.074 \pm 0.013$	3.0	$0.110 \pm 0.014$
2.5	$0.089 \pm 0.015$	5.0	$0.115 \pm 0.015$
3.5	$0.114 \pm 0.018$	7.0	$0.142 \pm 0.017$
4.5	$0.114 \pm 0.019$	9.0	$0.164 \pm 0.020$
5.5	$0.146 \pm 0.025$	11.0	$0.175 \pm 0.022$
6.5	$0.173 \pm 0.033$	13.0	$0.160 \pm 0.021$
7.5	$0.191 \pm 0.045$	15.0	$0.244 \pm 0.029$
8.5	$0.059 \pm 0.029$	17.0	$0.183 \pm 0.028$
9.5	$0.237 \pm 0.090$	19.0	$0.155 \pm 0.030$
10.5	$0.196 \pm 0.098$	21.0	$0.216 \pm 0.041$
—	—	23.0	$0.214 \pm 0.047$
—	—	25.0	$0.212 \pm 0.059$
—	—	27.0	$0.160 \pm 0.080$

## Figure Captions

Fig. 1. Differential cross section in the  $\eta$ -production angle for the  $pp \rightarrow pp\eta$  reaction at (a)  $Q = 37$  MeV ( $T_p = 1350$  MeV) and (b)  $Q = 16$  MeV ( $T_p = 1295$  MeV). The dashed curves represent the Monte Carlo predictions of phase space modified by the proton-proton final state interaction, whereas the solid curve includes also the angular dependence of Eq. (5) with  $a = -15$  and  $b = 22$ .

Fig. 2. Differential cross section in the proton-proton production angle for the  $pp \rightarrow pp\eta$  reaction at (a)  $Q = 37$  MeV and (b) 16 MeV with curves as described in Fig. 1.

Fig. 3. Distribution in  $\eta$  kinetic energies from the  $pp \rightarrow pp\eta$  reaction at (a)  $Q = 37$  MeV and (b) 16 MeV. The short-dashed curves represent the Monte Carlo predictions of phase space and the long-dashed shows the influence of the proton-proton final state interaction. The solid curve includes also the modifications induced by the angular and momentum dependence of Eq. (5) with  $a = -15$  and  $b = 22$ . Since the experimental acceptance changes somewhat according to the Monte Carlo generator used, the experimental points would be slightly lowered if we had extracted them using  $a = b = 0$ .

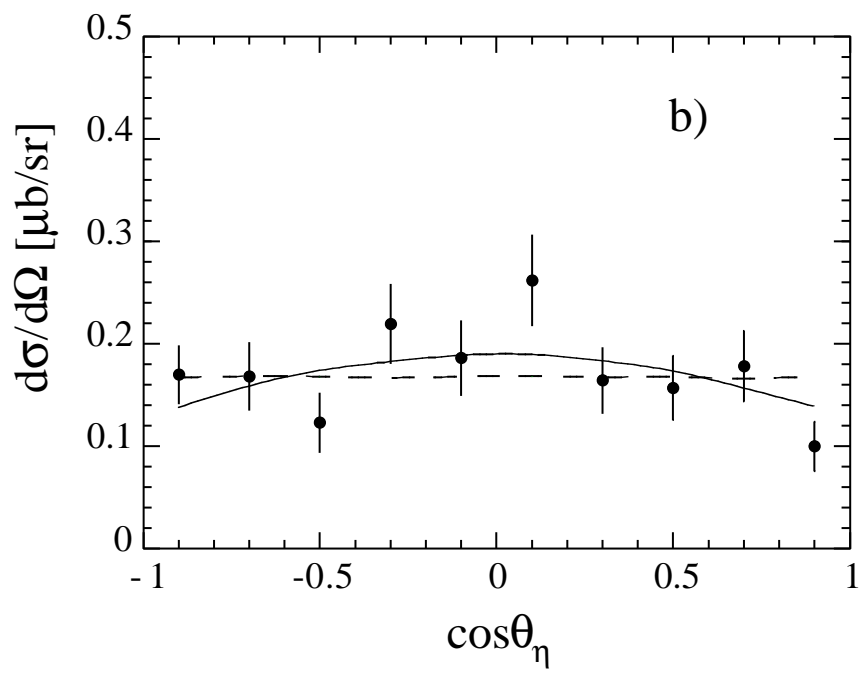
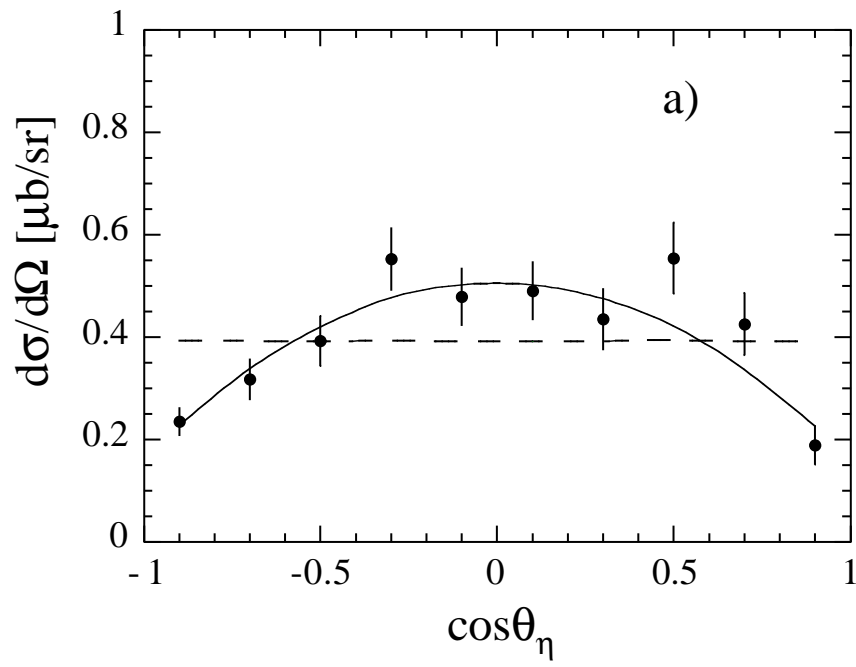


Figure 1

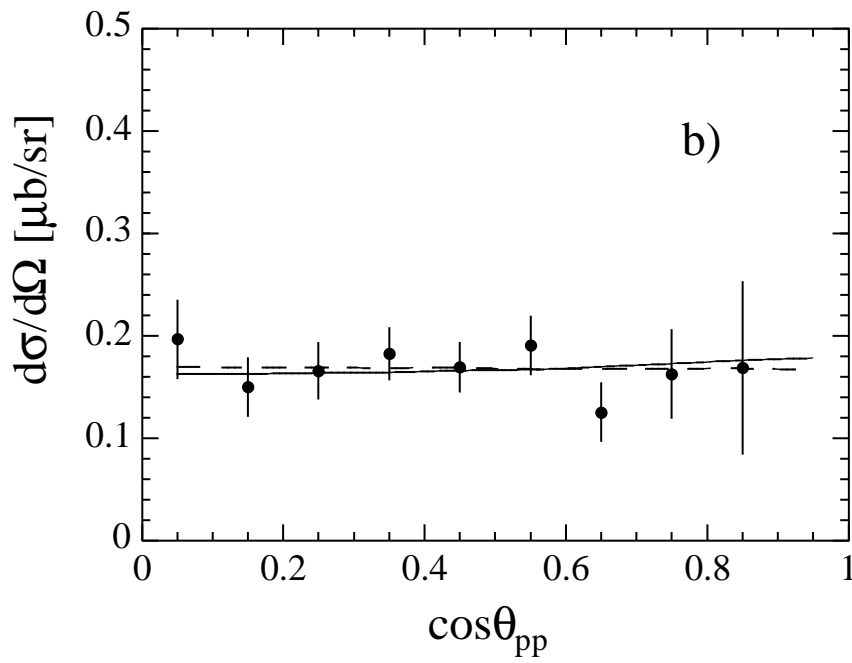
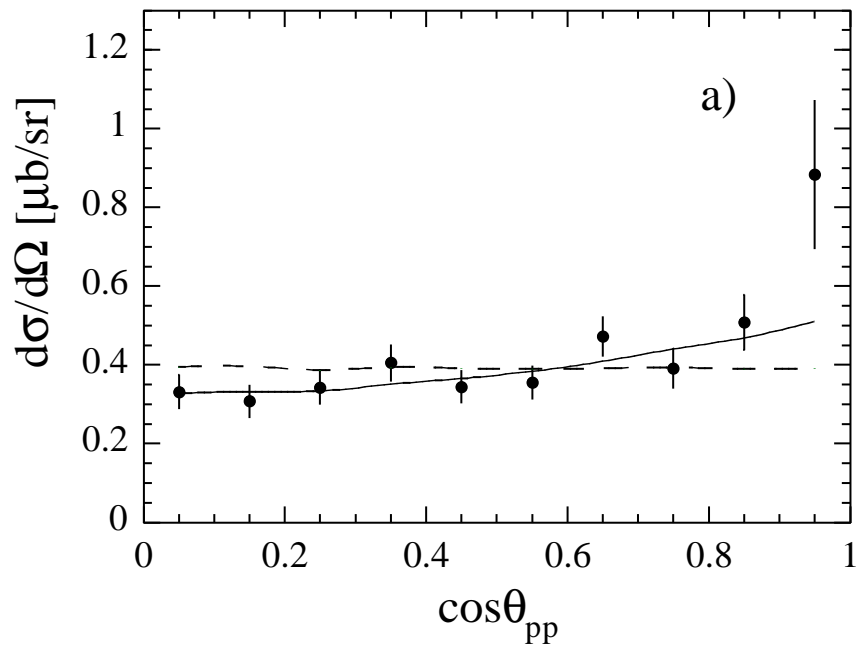


Figure 2



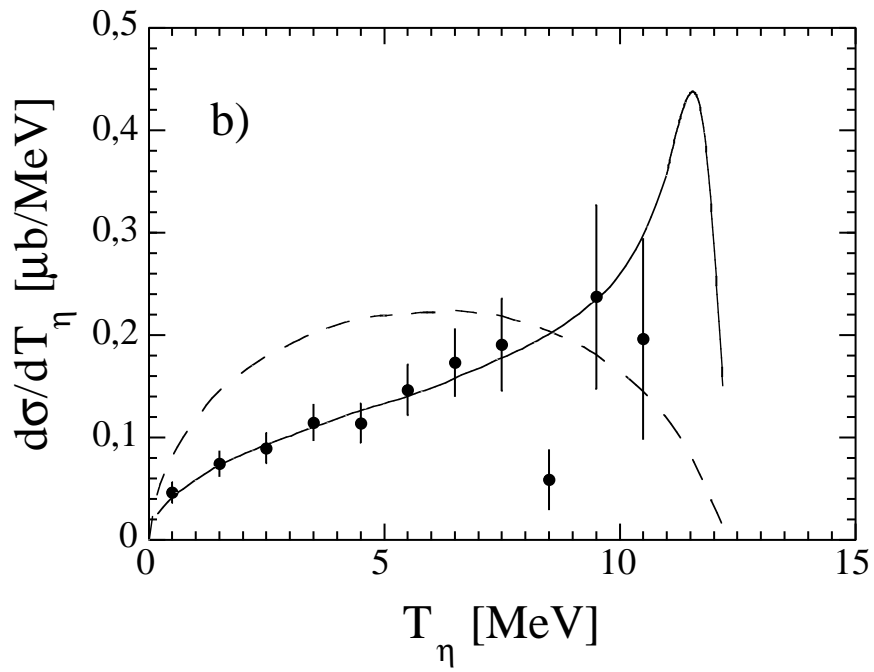
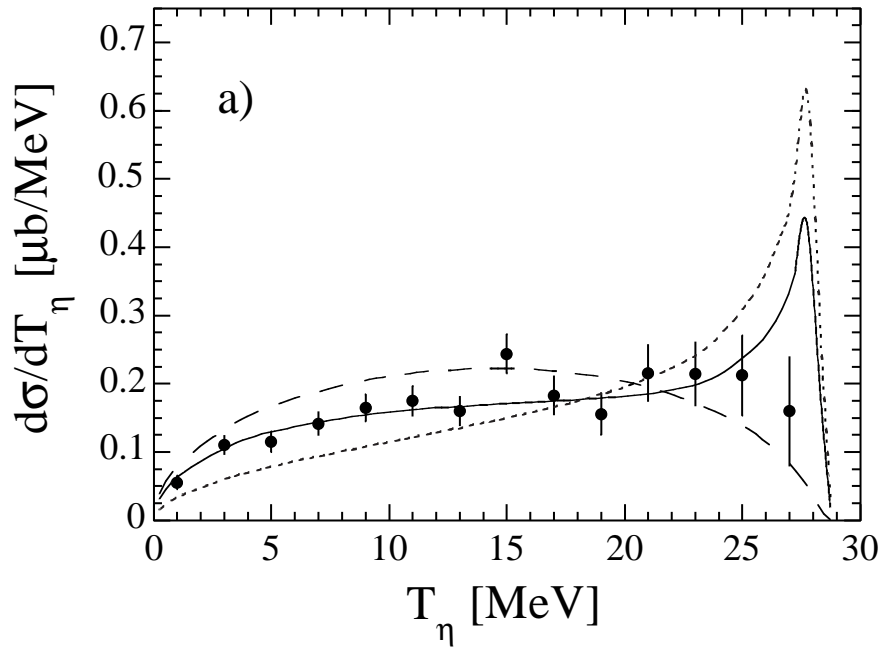


Figure 3